Precise measurement of the top quark mass in the dilepton channel at D0

V.M. Abazov,[35] B. Abbott,[73] B.S. Acharya,[29] M. Adams,[49] T. Adams,[47] G.D. Alexeev,[35] G. Alkhazov,[39] A. Alton[a],[61] G. Alverson,[60] G.A. Alves,[2] L.S. Ancu,[34] M. Aoki,[48] M. Arov,[58] A. Askew,[47] B. Åsman,[41] O. Atramentov,[65] C. Avila,[8] J. BackusMayes,[80] F. Badaud,[13] L. Bagby,[48] B. Baldin,[48] D.V. Bandurin,[47] S. Banerjee,[29] E. Barberis,[60] P. Baringer,[56] J. Barreto,[3] J.F. Bartlett,[48] U. Bassler,[18] V. Bazterra,[49] S. Beale,[6] A. Bean,[56] M. Begalli,[3] M. Begel,[71] C. Belanger-Champagne,[41] L. Bellantoni,[48] S.B. Beri,[27] G. Bernardi,[17] R. Bernhard,[22] I. Bertram,[42] M. Besançon,[18] R. Beuselinck,[43] V.A. Bezzubov,[38] P.C. Bhat,[48] V. Bhatnagar,[27] G. Blazey,[50] S. Blessing,[47] K. Bloom,[64] A. Boehnlein,[48] D. Boline,[70] E.E. Boos,[37] G. Borissov,[42] T. Bose,[59] A. Brandt,[76] O. Brandt,[23] R. Brock,[62] G. Brooijmans,[68] A. Bross,[48] D. Brown,[17] J. Brown,[17] X.B. Bu,[48] M. Buehler,[79] V. Buescher,[24] V. Bunichev,[37] S. Burdin[b],[42] T.H. Burnett,[80] C.P. Buszello,[41] B. Calpas,[15] E. Camacho-Pérez,[32] M.A. Carrasco-Lizarraga,[56] B.C.K. Casey,[48] H. Castilla-Valdez,[32] S. Chakrabarti,[70] D. Chakraborty,[50] K.M. Chan,[54] A. Chandra,[78] G. Chen,[56] S. Chevalier-Théry,[18] D.K. Cho,[75] S.W. Cho,[31] S. Choi,[31] B. Choudhary,[28] S. Cihangir,[48] D. Claes,[64] J. Clutter,[56] M. Cooke,[48] W.E. Cooper,[48] M. Corcoran,[78] F. Couderc,[18] M.-C. Cousinou,[15] A. Croc,[18] D. Cutts,[75] A. Das,[45] G. Davies,[43] K. De,[76] S.J. de Jong,[34] E. De La Cruz-Burelo,[32] F. Déliot,[18] M. Demarteau,[48] R. Demina,[69] D. Denisov,[48] S.P. Denisov,[38] S. Desai,[48] C. Deterre,[18] K. DeVaughan,[64] H.T. Diehl,[48] M. Diesburg,[48] A. Dominguez,[64] T. Dorland,[80] A. Dubey,[28] L.V. Dudko,[37] D. Duggan,[65] A. Duperrin,[15] S. Dutt,[27] A. Dyshkant,[50] M. Eads,[64] D. Edmunds,[62] J. Ellison,[46] V.D. Elvira,[48] Y. Enari,[17] H. Evans,[52] A. Evdokimov,[71] V.N. Evdokimov,[38] G. Facini,[60] T. Ferbel,[69] F. Fiedler,[24] F. Filthaut,[34] W. Fisher,[62] H.E. Fisk,[48] M. Fortner,[50] H. Fox,[42] S. Fuess,[48] A. Garcia-Bellido,[69] V. Gavrilov,[36] P. Gay,[13] W. Geng,[15,62] D. Gerbaudo,[66] C.E. Gerber,[49] Y. Gershtein,[65] G. Ginther,[48,69] G. Golovanov,[35] A. Goussiou,[80] P.D. Grannis,[70] S. Greder,[19] H. Greenlee,[48] Z.D. Greenwood,[58] E.M. Gregores,[4] G. Grenier,[20] Ph. Gris,[13] J.-F. Grivaz,[16] A. Grohsjean,[18] S. Grünendahl,[48] M.W. Grünewald,[30] T. Guillemin,[16] F. Guo,[70] G. Gutierrez,[48] P. Gutierrez,[73] A. Haas[c],[68] S. Hagopian,[47] J. Haley,[60] L. Han,[7] K. Harder,[44] A. Harel,[69] J.M. Hauptman,[55] J. Hays,[43] T. Head,[44] T. Hebbeker,[21] D. Hedin,[50] H. Hegab,[74] A.P. Heinson,[46] U. Heintz,[75] C. Hensel,[23] I. Heredia-De La Cruz,[32] K. Herner,[61] G. Hesketh[d],[44] M.D. Hildreth,[54] R. Hirosky,[79] T. Hoang,[47] J.D. Hobbs,[70] B. Hoeneisen,[12] M. Hohlfeld,[24] Z. Hubacek,[10,18] N. Huske,[17] V. Hynek,[10] I. Iashvili,[67] R. Illingworth,[48] A.S. Ito,[48] S. Jabeen,[75] M. Jaffré,[16] D. Jamin,[15] A. Jayasinghe,[73] R. Jesik,[43] K. Johns,[45] M. Johnson,[48] D. Johnston,[64] A. Jonckheere,[48] P. Jonsson,[43] J. Joshi,[27] A.W. Jung,[48] A. Juste,[40] K. Kaadze,[57] E. Kajfasz,[15] D. Karmanov,[37] P.A. Kasper,[48] I. Katsanos,[64] R. Kehoe,[77] S. Kermiche,[15] N. Khalatyan,[48] A. Khanov,[74] A. Kharchilava,[67] Y.N. Kharzheev,[35] D. Khatidze,[75] M.H. Kirby,[51] J.M. Kohli,[27] A.V. Kozelov,[38] J. Kraus,[62] S. Kulikov,[38] A. Kumar,[67] A. Kupco,[11] T. Kurča,[20] V.A. Kuzmin,[37] J. Kvita,[9] S. Lammers,[52] G. Landsberg,[75] P. Lebrun,[20] H.S. Lee,[31] S.W. Lee,[55] W.M. Lee,[48] J. Lellouch,[17] L. Li,[46] Q.Z. Li,[48] S.M. Lietti,[5] J.K. Lim,[31] D. Lincoln,[48] J. Linnemann,[62] V.V. Lipaev,[38] R. Lipton,[48] Y. Liu,[7] Z. Liu,[6] A. Lobodenko,[39] M. Lokajicek,[11] R. Lopes de Sa,[70] H.J. Lubatti,[80] R. Luna-Garcia[e],[32] A.L. Lyon,[48] A.K.A. Maciel,[2] D. Mackin,[78] R. Madar,[18] R. Magaña-Villalba,[32] S. Malik,[64] V.L. Malyshev,[35] Y. Maravin,[57] J. Martínez-Ortega,[32] R. McCarthy,[70] C.L. McGivern,[56] M.M. Meijer,[34] A. Melnitchouk,[63] D. Menezes,[50] P.G. Mercadante,[4] M. Merkin,[37] A. Meyer,[21] J. Meyer,[23] F. Miconi,[19] N.K. Mondal,[29] G.S. Muanza,[15] M. Mulhearn,[79] E. Nagy,[15] M. Naimuddin,[28] M. Narain,[75] R. Nayyar,[28] H.A. Neal,[61] J.P. Negret,[8] P. Neustroev,[39] S.F. Novaes,[5] T. Nunnemann,[25] G. Obrant,[39] J. Orduna,[78] N. Osman,[15] J. Osta,[54] G.J. Otero y Garzón,[1] M. Padilla,[46] A. Pal,[76] N. Parashar,[53] V. Parihar,[75] S.K. Park,[31] J. Parsons,[68] R. Partridge[c],[75] N. Parua,[52] A. Patwa,[71] B. Penning,[48] M. Perfilov,[37] K. Peters,[44] Y. Peters,[44] K. Petridis,[44] G. Petrillo,[69] P. Pétroff,[16] R. Piegaia,[1] J. Piper,[62] M.-A. Pleier,[71] P.L.M. Podesta-Lerma[f],[32] V.M. Podstavkov,[48] P. Polozov,[36] A.V. Popov,[38] M. Prewitt,[78] D. Price,[52] N. Prokopenko,[38] S. Protopopescu,[71] J. Qian,[61] A. Quadt,[23] B. Quinn,[63] M.S. Rangel,[2] K. Ranjan,[28] P.N. Ratoff,[42] I. Razumov,[38] P. Renkel,[77] M. Rijssenbeek,[70] I. Ripp-Baudot,[19] F. Rizatdinova,[74] M. Rominsky,[48] A. Ross,[42] C. Royon,[18] P. Rubinov,[48] R. Ruchti,[54] G. Safronov,[36] G. Sajot,[14] P. Salcido,[50] A. Sánchez-Hernández,[32] M.P. Sanders,[25] B. Sanghi,[48] A.S. Santos,[5] G. Savage,[48] L. Sawyer,[58] T. Scanlon,[43] R.D. Schamberger,[70] Y. Scheglov,[39] H. Schellman,[51] T. Schliephake,[26] S. Schlobohm,[80] C. Schwanenberger,[44] R. Schwienhorst,[62] J. Sekaric,[56] H. Severini,[73] E. Shabalina,[23] V. Shary,[18] A.A. Shchukin,[38] R.K. Shivpuri,[28]

Operated by Fermi Research Alliance, LLC under Contract No. DE-AC02-07CH11359 with the United States Department of Energy

V. Simak,[10] V. Sirotenko,[48] P. Skubic,[73] P. Slattery,[69] D. Smirnov,[54] K.J. Smith,[67] G.R. Snow,[64] J. Snow,[72] S. Snyder,[71] S. Söldner-Rembold,[44] L. Sonnenschein,[21] K. Soustruznik,[9] J. Stark,[14] V. Stolin,[36] D.A. Stoyanova,[38] M. Strauss,[73] D. Strom,[49] L. Stutte,[48] L. Suter,[44] P. Svoisky,[73] M. Takahashi,[44] A. Tanasijczuk,[1] W. Taylor,[6] M. Titov,[18] V.V. Tokmenin,[35] Y.-T. Tsai,[69] D. Tsybychev,[70] B. Tuchming,[18] C. Tully,[66] L. Uvarov,[39] S. Uvarov,[39] S. Uzunyan,[50] R. Van Kooten,[52] W.M. van Leeuwen,[33] N. Varelas,[49] E.W. Varnes,[45] I.A. Vasilyev,[38] P. Verdier,[20] L.S. Vertogradov,[35] M. Verzocchi,[48] M. Vesterinen,[44] D. Vilanova,[18] P. Vokac,[10] H.D. Wahl,[47] M.H.L.S. Wang,[69] J. Warchol,[54] G. Watts,[80] M. Wayne,[54] M. Weber[g,48] L. Welty-Rieger,[51] A. White,[76] D. Wicke,[26] M.R.J. Williams,[42] G.W. Wilson,[56] M. Wobisch,[58] D.R. Wood,[60] T.R. Wyatt,[44] Y. Xie,[48] C. Xu,[61] S. Yacoob,[51] R. Yamada,[48] W.-C. Yang,[44] T. Yasuda,[48] Y.A. Yatsunenko,[35] Z. Ye,[48] H. Yin,[48] K. Yip,[71] S.W. Youn,[48] J. Yu,[76] S. Zelitch,[79] T. Zhao,[80] B. Zhou,[61] J. Zhu,[61] M. Zielinski,[69] D. Zieminska,[52] and L. Zivkovic[75]

(The D0 Collaboration[*])

[1]*Universidad de Buenos Aires, Buenos Aires, Argentina*
[2]*LAFEX, Centro Brasileiro de Pesquisas Físicas, Rio de Janeiro, Brazil*
[3]*Universidade do Estado do Rio de Janeiro, Rio de Janeiro, Brazil*
[4]*Universidade Federal do ABC, Santo André, Brazil*
[5]*Instituto de Física Teórica, Universidade Estadual Paulista, São Paulo, Brazil*
[6]*Simon Fraser University, Vancouver, British Columbia, and York University, Toronto, Ontario, Canada*
[7]*University of Science and Technology of China, Hefei, People's Republic of China*
[8]*Universidad de los Andes, Bogotá, Colombia*
[9]*Charles University, Faculty of Mathematics and Physics, Center for Particle Physics, Prague, Czech Republic*
[10]*Czech Technical University in Prague, Prague, Czech Republic*
[11]*Center for Particle Physics, Institute of Physics, Academy of Sciences of the Czech Republic, Prague, Czech Republic*
[12]*Universidad San Francisco de Quito, Quito, Ecuador*
[13]*LPC, Université Blaise Pascal, CNRS/IN2P3, Clermont, France*
[14]*LPSC, Université Joseph Fourier Grenoble 1, CNRS/IN2P3, Institut National Polytechnique de Grenoble, Grenoble, France*
[15]*CPPM, Aix-Marseille Université, CNRS/IN2P3, Marseille, France*
[16]*LAL, Université Paris-Sud, CNRS/IN2P3, Orsay, France*
[17]*LPNHE, Universités Paris VI and VII, CNRS/IN2P3, Paris, France*
[18]*CEA, Irfu, SPP, Saclay, France*
[19]*IPHC, Université de Strasbourg, CNRS/IN2P3, Strasbourg, France*
[20]*IPNL, Université Lyon 1, CNRS/IN2P3, Villeurbanne, France and Université de Lyon, Lyon, France*
[21]*III. Physikalisches Institut A, RWTH Aachen University, Aachen, Germany*
[22]*Physikalisches Institut, Universität Freiburg, Freiburg, Germany*
[23]*II. Physikalisches Institut, Georg-August-Universität Göttingen, Göttingen, Germany*
[24]*Institut für Physik, Universität Mainz, Mainz, Germany*
[25]*Ludwig-Maximilians-Universität München, München, Germany*
[26]*Fachbereich Physik, Bergische Universität Wuppertal, Wuppertal, Germany*
[27]*Panjab University, Chandigarh, India*
[28]*Delhi University, Delhi, India*
[29]*Tata Institute of Fundamental Research, Mumbai, India*
[30]*University College Dublin, Dublin, Ireland*
[31]*Korea Detector Laboratory, Korea University, Seoul, Korea*
[32]*CINVESTAV, Mexico City, Mexico*
[33]*FOM-Institute NIKHEF and University of Amsterdam/NIKHEF, Amsterdam, The Netherlands*
[34]*Radboud University Nijmegen/NIKHEF, Nijmegen, The Netherlands*
[35]*Joint Institute for Nuclear Research, Dubna, Russia*
[36]*Institute for Theoretical and Experimental Physics, Moscow, Russia*
[37]*Moscow State University, Moscow, Russia*
[38]*Institute for High Energy Physics, Protvino, Russia*
[39]*Petersburg Nuclear Physics Institute, St. Petersburg, Russia*
[40]*Institució Catalana de Recerca i Estudis Avançats (ICREA) and Institut de Física d'Altes Energies (IFAE), Barcelona, Spain*
[41]*Stockholm University, Stockholm and Uppsala University, Uppsala, Sweden*
[42]*Lancaster University, Lancaster LA1 4YB, United Kingdom*
[43]*Imperial College London, London SW7 2AZ, United Kingdom*
[44]*The University of Manchester, Manchester M13 9PL, United Kingdom*
[45]*University of Arizona, Tucson, Arizona 85721, USA*
[46]*University of California Riverside, Riverside, California 92521, USA*
[47]*Florida State University, Tallahassee, Florida 32306, USA*

[48]Fermi National Accelerator Laboratory, Batavia, Illinois 60510, USA
[49]University of Illinois at Chicago, Chicago, Illinois 60607, USA
[50]Northern Illinois University, DeKalb, Illinois 60115, USA
[51]Northwestern University, Evanston, Illinois 60208, USA
[52]Indiana University, Bloomington, Indiana 47405, USA
[53]Purdue University Calumet, Hammond, Indiana 46323, USA
[54]University of Notre Dame, Notre Dame, Indiana 46556, USA
[55]Iowa State University, Ames, Iowa 50011, USA
[56]University of Kansas, Lawrence, Kansas 66045, USA
[57]Kansas State University, Manhattan, Kansas 66506, USA
[58]Louisiana Tech University, Ruston, Louisiana 71272, USA
[59]Boston University, Boston, Massachusetts 02215, USA
[60]Northeastern University, Boston, Massachusetts 02115, USA
[61]University of Michigan, Ann Arbor, Michigan 48109, USA
[62]Michigan State University, East Lansing, Michigan 48824, USA
[63]University of Mississippi, University, Mississippi 38677, USA
[64]University of Nebraska, Lincoln, Nebraska 68588, USA
[65]Rutgers University, Piscataway, New Jersey 08855, USA
[66]Princeton University, Princeton, New Jersey 08544, USA
[67]State University of New York, Buffalo, New York 14260, USA
[68]Columbia University, New York, New York 10027, USA
[69]University of Rochester, Rochester, New York 14627, USA
[70]State University of New York, Stony Brook, New York 11794, USA
[71]Brookhaven National Laboratory, Upton, New York 11973, USA
[72]Langston University, Langston, Oklahoma 73050, USA
[73]University of Oklahoma, Norman, Oklahoma 73019, USA
[74]Oklahoma State University, Stillwater, Oklahoma 74078, USA
[75]Brown University, Providence, Rhode Island 02912, USA
[76]University of Texas, Arlington, Texas 76019, USA
[77]Southern Methodist University, Dallas, Texas 75275, USA
[78]Rice University, Houston, Texas 77005, USA
[79]University of Virginia, Charlottesville, Virginia 22901, USA
[80]University of Washington, Seattle, Washington 98195, USA

(Dated: April 28, 2011)

We measure the top quark mass (m_t) in $p\bar{p}$ collisions at a center of mass energy $\sqrt{s} = 1.96$ TeV using dilepton $t\bar{t} \to W^+bW^-\bar{b} \to \ell^+\nu_\ell b\ell^-\bar{\nu}_\ell\bar{b}$ events, where ℓ denotes an electron, a muon, or a tau lepton that decays leptonically. The data correspond to an integrated luminosity of 5.4 fb^{-1} collected with the D0 detector at the Fermilab Tevatron Collider. We obtain $m_t = 174.0 \pm 1.8(\text{stat}) \pm 2.4(\text{syst})$ GeV, which is in agreement with the current world average $m_t = 173.3 \pm 1.1$ GeV. This is currently the most precise measurement of m_t in the dilepton channel.

PACS numbers: 14.65.Hz

The measurement of the properties of the top quark has been a major goal of the Fermilab Tevatron Collider experiments since its discovery in 1995 [1, 2]. As the heaviest known elementary particle, the top quark may play a special role in the mechanism of electroweak symmetry breaking. A precise measurement of its mass (m_t) is of particular importance, since, combined with the measurement of the W boson mass, it provides an indirect constraint on the mass of the Higgs boson in the standard model (SM), and can also constrain possible extensions of the SM.

We present a new measurement of the top quark mass in the dilepton channel (ee, $e\mu$, $\mu\mu$) in $t\bar{t} \to W^+bW^-\bar{b} \to \ell^+\nu_\ell b\ell^-\bar{\nu}_\ell\bar{b}$ events, where ℓ denotes an electron, a muon or a tau decaying leptonically, using the matrix element (ME) method. The first measurement of m_t based on this method was performed in the lepton+jets channel by the D0 experiment [3]. The CDF collaboration has applied the ME approach to determine m_t in the dilepton and all-hadronic final states [4, 5], obtaining a mass precision of 4.0 GeV for dilepton events [4]. The measurement of m_t in the dilepton channel has also been carried out using other techniques [6–10], reaching a precision of 4.8 GeV. We report a measurement based on data collected by the D0 detector, corresponding to 5.4 fb^{-1} of integrated luminosity from $p\bar{p}$ collisions at $\sqrt{s} = 1.96$ TeV.

*with visitors from [a]Augustana College, Sioux Falls, SD, USA, [b]The University of Liverpool, Liverpool, UK, [c]SLAC, Menlo Park, CA, USA, [d]University College London, London, UK, [e]Centro de Investigacion en Computacion - IPN, Mexico City, Mexico, [f]ECFM, Universidad Autonoma de Sinaloa, Culiacán, Mexico, and [g]Universität Bern, Bern, Switzerland.

The D0 detector has a central tracking system, consisting of a silicon microstrip tracker and a central fiber tracker, both located within a 1.9 T superconducting solenoidal magnet [11], with design providing tracking and vertexing at pseudorapidities $|\eta| < 3$ [12]. The liquid-argon and uranium calorimeter has a central section (CC) covering pseudorapidities $|\eta|$ up to ≈ 1.1 and two end calorimeters (EC) that extend coverage to $|\eta| \approx 4.2$, with all three housed in separate cryostats [13]. A muon system outside the calorimeters covers $|\eta| < 2$ and consists of a layer of tracking detectors and scintillation trigger counters in front of 1.8 T toroids, followed by two similar layers after the toroids [14].

Despite the small branching fraction of this final state and the presence of two neutrinos in each event, the measurement of m_t in the dilepton channel is interesting because the lower background and the smaller jet multiplicity relative to the lepton+jets channel result in a reduced sensitivity to the ambiguity from combining jets in the reconstruction of m_t. The dilepton measurement therefore complements the results from other final states. Moreover, significant differences in measured values of m_t in different $t\bar{t}$ decay channels can be indicative of the presence of physics beyond the SM [15].

As the SM predicts top quarks to decay almost 100% of the time into a W boson and a b quark, $t\bar{t}$ events are classified according to the decays of the W boson. In the dilepton channel, both W bosons decay leptonically, $W^+ \to \ell^+\nu_\ell$ [16] with $\ell = e, \mu$ or τ. We analyze the events characterized by two leptons ee, $e\mu$, or $\mu\mu$, with a large transverse momenta (p_T), large imbalance in transverse momentum from the undetected neutrinos ($\not{p}_T$), and two high-p_T jets from the b quarks. The $W^+ \to \tau^+\nu_\tau$ decays contribute through secondary $\tau^+ \to \ell^+\nu_\ell\bar{\nu}_\tau$ transitions.

For the ee and $\mu\mu$ analysis, we consider events selected by a set of single-lepton triggers. For the $e\mu$ channel, we use a mixture of single and multilepton triggers and lepton+jet triggers. Dilepton $t\bar{t}$ events are required to have at least two oppositely charged, isolated leptons with $p_T > 15$ GeV, and either $|\eta| < 1.1$ or $1.5 < |\eta| < 2.5$ for electrons and $|\eta| < 2$ for muons. If more than one lepton-pair combination is found in an event, only the pair with the largest sum in scalar p_T is used. Events must have at least two jets with $p_T > 20$ GeV and $|\eta| < 2.5$, well separated from the selected electrons. No explicit b jet identification is required in this analysis.

The main sources of background in the dilepton channel are Drell-Yan and Z boson production ($Z/\gamma^* \to \ell^+\ell^-$), diboson production ($WW, WZ, ZZ$), and instrumental background that originates from limited detector resolution and lepton misidentification. In the ee channel, the discrimination between the $t\bar{t}$ signal and background improves by requiring a large significance of the measured $\not{p}_T$, which is defined through a likelihood discriminant constructed from the ratio of $\not{p}_T$ to its uncertainty [17]. In the $\mu\mu$ channel, we require, in addition, $\not{p}_T > 40$ GeV. In the $e\mu$ channel, the requirement $H_T > 115$ GeV, where H_T is the scalar sum of the transverse momenta of the leading lepton and the two leading jets, rejects most of the contribution from $\tau^+ \to \ell^+\nu_\ell\bar{\nu}_\tau$. The above selections minimize the expected statistical uncertainty on m_t. In total, we select 479 candidate events with 73, 266, and 140 events, respectively, in the ee, $e\mu$, and $\mu\mu$ channels, of which about 13 ± 5, 48 ± 15, and 56 ± 15 events, respectively, are expected to arise from background.

The matrix element method is based on the probability for a given event to resemble signal, which depends on the value of m_t, or background, which is usually independent of m_t. Assuming that the different physics processes leading to the same final state do not interfere, the event probability can be written as the sum of probabilities from all possible contributions. In practice, because the ME method requires significant computing time, only the dominant background is taken into account, and the total event probability is given by

$$P_{\rm evt} = f_{t\bar{t}} P_{t\bar{t}}(x; m_t) + (1 - f_{t\bar{t}}) P_{Z+2\ {\rm jets}}(x), \qquad (1)$$

where $f_{t\bar{t}}$ is the fraction of $t\bar{t}$ events, $P_{t\bar{t}}$ and $P_{Z+2\ {\rm jets}}$ are the signal and background probability densities, respectively, m_t is the assumed top quark mass, and x reflects the observed kinematic variables, i.e., the four-momenta of the measured jets and leptons. In the ee, $\mu\mu$, and $e\mu$ channels, $Z+2$ jets events with $Z \to e^+e^-$,$Z \to \mu^+\mu^-$ and $Z \to \tau^+\tau^- \to e^+\nu_e\mu^-\bar{\nu}_\mu$) are expected to be the dominant source of background. There is no bias expected from neglecting other background probabilities, as the analysis is calibrated using all significant sources of background, which provides a way to correct for the limitations of the model, as described below.

The leading-order (LO) matrix element for $q\bar{q} \to t\bar{t} \to W^+bW^-\bar{b} \to \ell^+\nu_\ell b\ell^-\bar{\nu}_\ell\bar{b}$ is used to compute the $t\bar{t}$ probability density. For each final state y of the six produced partons, the signal probability is given by

$$\begin{aligned} P_{t\bar{t}}(x; m_t) = & \frac{1}{\sigma_{\rm obs}(m_t)} \\ & \cdot \sum_{i=1}^{8} \int {\rm d}q_1\ {\rm d}q_2\ f_{\rm PDF}(q_1)\ f_{\rm PDF}(q_2) \qquad (2) \\ & \cdot \frac{(2\pi)^4\, |M(y)|^2}{q_1 q_2 s}\ {\rm d}\Phi_6\ W(x,y)\ W(p_T^{t\bar{t}})\ , \end{aligned}$$

where q_1, q_2 denote the momentum fractions of the incident quarks in the proton and antiproton, $f_{\rm PDF}$ are the parton distribution functions (PDF) for finding a parton of a given flavor and longitudinal momentum fraction in the proton or antiproton (in this analysis we use the CTEQ6L1 PDF [18]), s is the square of the energy in the $q\bar{q}$ rest frame, $M(y)$ is the leading-order matrix element [19] and ${\rm d}\Phi_6$ is an element of the 6-body phase space. Detector resolution is taken into account through a transfer function $W(x, y)$ that describes the probability of the partonic final state y to be measured as x in the detector. The finite transverse momentum of the $t\bar{t}$ system is accounted for through an integration over its probability distribution, which is derived from parton-level simulated events using the ALPGEN event generator [20], employing PYTHIA [21] for parton shower development and hadronization. As the angular resolution of the jets and leptons, as well as the electron energy resolution, are sufficiently well determined, there is no need to introduce resolution functions for these variables. Consequently, taking into account energy and momentum conservation, the integration in Eq. (2) can be reduced to an integration over the energies associated with the b quarks, the lepton-neutrino invariant masses, the differences between neutrino transverse momenta, the transverse momentum of the $t\bar{t}$ system, and the radii of curvature (p_T^{-1}) of muons. The sum in Eq. (2) runs over both possible jet-parton assignments and over up to two real solutions for each neutrino energy [22]. The normalization factor $\sigma_{\rm obs}$ in Eq. (2) corresponds to the product of the LO cross section and the mean efficiency of the final kinematic selections.

A transfer function $W(x, y)$ is used for each jet and each muon in the final state. The jet energy resolution is parametrized as the sum of two Gaussians, with parameters depending linearly on parton energies, while the resolution in muon track curvature is described by a single Gaussian. All parameters in $W(x, y)$ are determined from simulated Monte Carlo (MC) $t\bar{t}$ events, tuned to match the resolutions observed in data.

To take account of all individual background processes and to provide a correct statistical sampling of possible spin, flavor, and color configurations, the background probability $P_{Z+2\text{ jets}}$ is calculated using VECBOS [23]. Since $Z \to \tau^+\tau^-$ decay is not modeled in VECBOS, an additional transfer function in the $e\mu$ channel is used to describe the energy of the final state lepton relative to the initial τ lepton, and is derived from parton-level information [22]. The direction of the final state lepton is assumed to be close to that of the original τ lepton, since only in such cases the lepton from the τ decay is sufficiently energetic to pass the lepton p_T selection. For the $(Z \to \tau^+\tau^- \to e^+\nu_e\mu^-\bar{\nu}_\mu)$+2 jets probability, the energy fractions for final state leptons are sampled according to this τ transfer function. Just as for the case of the signal probabilities, the jet and charged-lepton directions are assumed to be well-measured, and each kinematic solution is weighted according to the p_T of the $Z + 2$ jets system. The integration of the probability for $Z+2$ jets is performed over the energies of the two partons that lead to the jets. Both possible assignments of jets to quarks are considered in this analysis.

To calculate the signal and background probability densities, a MC-based integration of Eq. (2) is performed and m_t is changed in steps of 2.5 GeV over a range of 30 GeV. For each mass hypothesis, a likelihood function $L_{\rm tot}(m_t, f_{t\bar{t}})$ is defined by the product of individual event probabilities $P_{\rm evt}$, and the signal fraction $f_{t\bar{t}}$ is determined by minimizing $-\ln L_{\rm tot}$. Finally, the most likely value of m_t and its uncertainty are extracted from a fit of $L_{\rm tot}(m_t)$ to a Gaussian form near its maximum using the value of $f_{t\bar{t}}$ found in the previous step.

To check for any bias caused by approximations of the method, such as the use of the LO matrix element for $P_{t\bar{t}}$ or from neglecting backgrounds other than $Z + 2$ jets, the measurement is calibrated using MC events generated with ALPGEN + PYTHIA. All events are processed through a full GEANT3 [24] detector simulation, followed by the same reconstruction and analysis chain as used for data. Effects from additional $p\bar{p}$ interactions are simulated by overlaying data from random $p\bar{p}$ crossings over the MC events.

Five $t\bar{t}$ MC samples are generated with input top quark masses of $m_t = 165$, 170, 172.5, 175, and 180 GeV. Probabilities for the $t\bar{t}$ signal and for $Z/\gamma^* \to \ell^+\ell^-$, diboson and instrumental backgrounds, are used to form randomly drawn pseudo-experiments. The total number of events in each pseudo-experiment is fixed to the number of events in data for the combined dilepton channels. The signal and background fractions are fluctuated according to multinomial statistics around the fractions determined from the measured $t\bar{t}$ cross section in the separate channels [25].

The mean values of m_t measured in 1,000 pseudo-experiments as a function of the input m_t are shown in Fig. 1(a). The deviation from the ideal response, where the extracted mass corresponds to the input mass, is caused by the presence of background. For the case of background-free pseudo-experiments, no difference is observed. The width of the distribution of the pulls ("pull width"), defined as the mean deviation of m_t in single pseudo-experiments from the mean for all 1,000 values at a given input m_t, in units of the measured uncertainty per pseudo-experiment, is shown in Fig. 1(b). The statistical uncertainty measured in data is corrected for the deviation of the pull width from unity. The calibrated value of m_t from the fit to the data is shown in Fig. 2(a). Figure 2(b) compares the measured uncertainty for m_t with the distribution of expected uncertainties in pseudo-experiments at $m_t = 175$ GeV.

Systematic uncertainties on the measurement of m_t can be divided into three categories. The first involves uncertainties from modeling of the detector, such as the uncertainty on the energy scale of light-quark jets, the uncertainty in the relative calorimeter response to b and light-quark jets, as well as in the energy resolution for jets, muons, and electrons. The second category is related to the modeling of $t\bar{t}$ production. This includes possible differences in the amount of initial and final state radiation, effects from next-to-leading order contributions and different hadronization models, color reconnection, and modeling of b-quark fragmentation as well as uncertainties from choice of PDF. The third category comprises effects from calibration, such as the uncertainties in the calibration function shown in Fig. 1(a), and from variations in signal and background contributions in the pseudo-experiments. Contributions to the total systematic uncertainty in the measurement of m_t are summarized in Table I.

The dominant systematic uncertainty in the dilepton channel is from the difference in detector response between light and b-quark jets that is estimated by propagating the difference in response of single pions in data and MC to the jet energy scale of jets arising from b quarks. The next important uncertainty arises from uncertainties in the global jet energy scale of light quarks (JES). This jet energy scale is calibrated using γ+jets and dijet data events [26]. It has a total uncertainty of typically 2% per jet, which translates into an uncertainty on m_t of 1.5 GeV. The main systematic uncertainty from modeling $t\bar{t}$ production is from higher-order effects and hadronization. This uncertainty is evaluated by using $t\bar{t}$ events generated with MC@NLO [27] and evolved in HERWIG [28]. The next leading uncertainty on modeling $t\bar{t}$ arises from the modeling of b quark fragmentation. It is derived by comparing the extracted m_t for the default measurement with the result using a re-weighting of the default MC samples to a Bowler scheme tuned to LEP or SLD data [29]. The largest difference is quoted as the uncertainty.

In summary, we have presented a measurement of the mass of the top quark in the $t\bar{t} \rightarrow W^+bW^-\bar{b} \rightarrow \ell^+\nu_\ell b\ell^-\bar{\nu}_\ell\bar{b}$ channel using the matrix element method. Based on an integrated luminosity of 5.4 fb^{-1} collected by the D0 collaboration, the top quark mass is found to be

$$m_t = 174.0 \pm 1.8(\text{stat}) \pm 2.4(\text{syst}) \text{ GeV}. \tag{3}$$

This measurement is in good agreement with the current world average $m_t = 173.3 \pm 1.1$ GeV [30]. Its total uncertainty of 3.1 GeV corresponds to a 1.8 % accuracy, and represents the most precise measurement of m_t from dilepton $t\bar{t}$ final states.

We thank the staffs at Fermilab and collaborating institutions, and acknowledge support from the DOE and NSF (USA); CEA and CNRS/IN2P3 (France); FASI, Rosatom and RFBR (Russia); CNPq, FAPERJ, FAPESP and FUNDUNESP (Brazil); DAE and DST (India); Colciencias (Colombia); CONACyT (Mexico); KRF and KOSEF (Korea); CONICET and UBACyT (Argentina); FOM (The Netherlands); STFC and the Royal Society (United Kingdom); MSMT and GACR (Czech Republic); CRC Program and NSERC (Canada); BMBF and DFG (Germany); SFI (Ireland); The Swedish Research Council (Sweden); and CAS and CNSF (China).

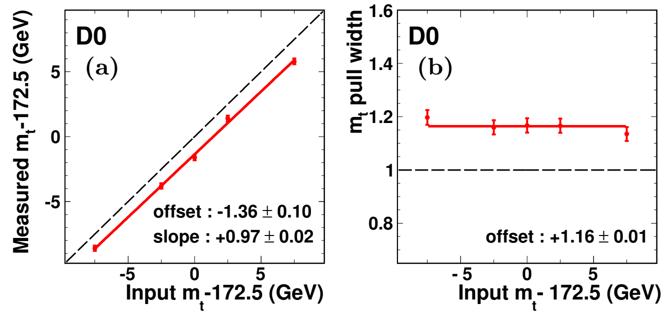

FIG. 1: (a) Mean values of m_t and (b) pull width from sets of 1,000 pseudo-experiments as a function of input m_t for the combined dilepton channels. The dashed lines represent the ideal response in (a), where the extracted mass is identical to the input mass, and in (b), where the statistical uncertainty requires no correction.

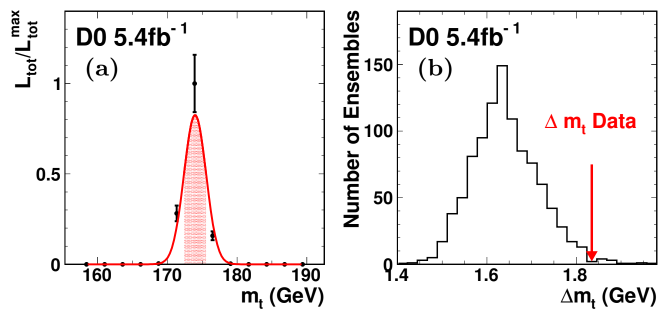

FIG. 2: Combined for all channels: (a) Calibrated and normalized likelihood for data as a function of m_t with best estimate as well as 68% confidence level region marked by the shated area and in (b) the expected distribution of uncertainties with the measured uncertainty indicated by the arrow. As the top quark mass is measured to be $m_t = 174.0$ GeV, the expected distribution in (b) is shown for the closest input mass $m_t = 175$ GeV used in the pseudo-experiment.

[1] F. Abe *et al.* (CDF Collaboration), Phys. Rev. Lett. **74**, 2626 (1995).
[2] S. Abachi *et al.* (D0 Collaboration), Phys. Rev. Lett. **74**, 2632 (1995).
[3] V. M. Abazov *et al.* (D0 Collaboration), Nature **429**, 638 (2004).
[4] A. Abulencia *et al.* (CDF Collaboration), Phys. Rev. Lett. **102**, 152001 (2007).
[5] A. Aaltonen *et al.* (CDF Collaboration), Phys. Rev. D **79**, 072010 (2009).
[6] A. Aaltonen *et al.* (CDF Collaboration), Phys. Rev. Lett. **100**, 062005 (2008).
[7] A. Aaltonen *et al.* (CDF Collaboration), Phys. Rev. D **79**, 092005 (2009).
[8] A. Aaltonen *et al.* (CDF Collaboration), Phys. Rev. D **79**, 072005 (2009).
[9] V. M. Abazov *et al.* (D0 Collaboration), Phys. Lett. B

TABLE I: Summary of systematic uncertainties on the measurement of m_t in dilepton events.

Source	Uncertainty (GeV)
Detector modeling:	
b/light jet response	± 1.6
JES	± 1.5
Jet resolution	± 0.3
Muon resolution	± 0.2
Electron p_T scale	± 0.4
Muon p_T scale	± 0.2
ISR/FSR	± 0.2
Signal modeling:	
Higher order and hadronization	± 0.7
Color reconnection	± 0.1
b-quark modeling	± 0.4
PDF uncertainty	± 0.1
Method:	
MC calibration	± 0.1
Signal fraction	± 0.5
Total	± 2.4

655, 7 (2009).

[10] V. M. Abazov *et al.* (D0 Collaboration), Phys. Rev. D **80**, 092006 (2009).

[11] V. M. Abazov *et al.* (D0 Collaboration), Nucl. Instrum. Meth. Phys. Res. A **565**, 463 (2006).

[12] The pseudorapidity η is defined relative to the center of the detector as $\eta = -\ln[\tan(\theta/2)]$ where θ is the polar angle with respect to the proton beam direction.

[13] S. Abachi *et al.* (D0 Collaboration), Nucl. Instrum. Meth. Phys. Res. A **338**, 185 (1994).

[14] V. M. Abazov *et al.* (D0 Collaboration), Nucl. Instrum. Meth. Phys. Res. A **552**, 372 (2005).

[15] G. L. Kane and S. Mrenna, Phys. Rev. Lett. **77**, 3502 (1996).

[16] Throughout this Letter, charge conjugated processes are included implicitly.

[17] A. G. Schwartzman, FERMILAB-THESIS-2004-21.

[18] J. Pumplin *et al.*, J. High Energy Phys. **07** 012 (2002).

[19] G. Mahlon and S. Parke, Phys. Lett. B **411** 173 (1997).

[20] M. L. Mangano, M. Moretti, F. Piccinini, R. Pittau, and A. D. Polosa, J. High Energy Phys. **07**, 001 (2003).

[21] T. Sjöstrand, S. Mrenna, P. Skands, J. High Energy Phys. **05** 026 (2006).

[22] F. Fiedler, A. Grohsjean, P. Haefner, and P. Schieferdecker, Nucl. Instrum. Meth. Phys. Res. A **624**, 203 (2010).

[23] F. A. Berends, H. Kuijf, B. Tausk, and W. T. Giele, Nucl. Phys. **B 357**, 32 (1991).

[24] R. Brun, F. Carminati, CERN Program Library Long Writeup W5013, 1993 (unpublished).

[25] V. M. Abazov *et al.* (D0 Collaboration), arXiv:hep-ex/1103.1871, submitted to Phys. Lett. B

[26] V. M. Abazov *et al.* (D0 Collaboration), Phys. Rev. Lett. **101**, 062001 (2008).

[27] S. Frixione and B. R. Webber, arXiv:hep-ph/0612272.

[28] G. Corcella *et al.* J. High Energy Phys. **01**, 010 (2001).

[29] The ALEPH Collaboration, the DELPHI Collaboration, the L3 Collaboration, the OPAL Collaboration, the SLD Collaboration, the LEP Electroweak Working Group, the SLD electroweak, heavy-flavor groups, arXiv:hep-ex/0509008.

[30] The Tevatron Electroweak Working Group (CDF and D0 Collaborations), arXiv:1007.3178 [hep-ex] (2010).